Atom Probe Field Ion Microscopy Study of the Partitioning of Substitutional Elements during Tempering of a Low-Alloy Steel Martensite

S.S. BABU, K. HONO, and T. SAKURAI

The partitioning behavior of Mn and Si at the cementite/ferrite interface during tempering of Fe-C-Si-Mn steel martensite has been studied by atom probe field-ion microscopy (APFIM). It has been shown that cementite can form without partitioning of Si and Mn during the early tempering stage at a low temperature. The atom probe compositional analysis shows no evidence of segregation or of concentration spikes of substitutional elements at the interface. This suggests that the early stage of cementite growth occurs by paraequilibrium mode and is controlled only by C diffusion in the matrix. In addition, significant C concentration fluctuations are measured in the as-quenched condition. The onset of partitioning of both Si and Mn occurs after prolonged time or by increasing the tempering temperature.

I. INTRODUCTION

THE kinetic models of reconstructive growth in low-alloy steels aim to predict the interface velocity, volume fraction, and composition of product phases as a function of alloy composition, transformation temperature, and time. Theories of reconstructive transformations in ternary steels are already available.[1–8] These theories have been extensively used to model the reconstructive transformation of austenite to ferrite in low-alloy steels.[9,10] Nevertheless, the theories are general and can be applied to any situation involving reconstructive growth of a precipitate phase. In these kinetic models, *local equilibrium* at the interphase interface is assumed for predicting velocities of transformation interfaces. With the local equilibrium assumption, three transformation modes were proposed for the transformations in steels involving the diffusion of both substitutional and interstitial elements. In low supersaturation and low interface velocity, the transformation is controlled by the slow diffuser (substitutional elements) and the local equilibrium at interface exists. This mode is known as *partitioning local equilibrium* (PLE). In high supersaturation and high interface velocity, the transformation is controlled by the fast diffuser (interstitial atoms) and the local equilibrium at the interface exists. This mode is known as *negligible partitioning local equilibrium* (NPLE). In NPLE mode, a steep concentration gradient of substitutional element, which is known as a diffusion spike, is assumed in front of the growing interface.[4]

The estimated width of these diffusion spikes reduces as a function of undercooling. In very high undercoolings, the diffusion-spike width reduces to the order of atomic spacing. In this condition, it is assumed that the local equilibrium fails and the transformation mode switches to paraequilibrium.[4,7–11] In the paraequilibrium condition, there is no redistribution of substitutional elements between the precipitated phase and the matrix. The ratio of Fe/X (X = substitutional elements) concentration remains constant at both sides of the interface. Paraequilibrium growth is possible if C reaches its equilibrium concentration in both parent and product phases.[4–8] In this case, the growth of the product phase is controlled only by C diffusion. Several experimental works were conducted to determine the partitioning of substitutional elements under the paraequilibrium reaction by employing electron probe microanalysis and analytical electron microscopy.[9,10] However, because of the insufficient spatial resolution of the conventional analytical techniques, the most critical information on the interfacial concentration of alloying elements during the growth of precipitates has not been available. Moreover, there is no satisfactory theory for the transition from paraequilibrium to local equilibrium during the growth of the precipitates.[11]

The previous theoretical works on paraequilibrium were proposed for ferrite and pearlite reaction in steels;[1–6] however, paraequilibrium is also applicable to the precipitation of cementite from low-alloy steel martensite. According to equilibrium thermodynamics, the solid solubility of Si in cementite is almost zero, and Mn has high solid solubility in cementite. The expected concentration-depth profiles for cementite growth from martensite for all three transformation modes are schematically illustrated in Figure 1. The tempering of martensite steels is usually carried out in low temperatures, where the diffusivity of C is many orders of magnitude greater than the diffusivity of substitutional elements; *e.g.*, $D_{Si} \approx D_{Mn} \approx 10^{-20}$ cm^2 s^{-1}; and $D_C \approx 10^{-9}$ cm^2 s^{-1} at 350 °C.[13,14] Thus, the precipitation of cementite may proceed either by NPLE mode (Figure 1(b)) or paraequilibrium mode (Figure 1(c)) in the early stages of tempering. Kinetic models are not sufficient to predict which mode would actually control the growth of cementite in the present low-alloy steel. Hence, it is interesting to determine the transformation mode experimentally by measuring the concentration of cementite/ferrite (θ/α) interface.

S.S. BABU, formerly Research Associate, Institute for Materials Research, Tohoku University, is Postdoctoral Research Associate, Metals and Ceramics Division, Oak Ridge National Laboratory, Oak Ridge, TN 37830. K. HONO, Research Associate, and T. SAKURAI, Professor, are with the Institute for Materials Research, Tohoku University, Sendai 980, Japan.

Manuscript submitted April 12, 1993.

The aim of this study is to determine the concentration of solute elements at the θ/α interface during early-stage tempering of Fe-C-Si-Mn martensite. It should be noted that measurement of bulk compositions of parent and product phases is not sufficient to distinguish between the NPLE and paraequilibrium modes. The NPLE mode is associated with thin diffusion spikes of substitutional elements at the interface. On the other hand, in paraequilibrium mode, diffusion spikes are not expected at the interface. The concentrations of the solute elements between the product and parent phases are the same in both cases. Since conventional analytical techniques cannot resolve the variation of chemical concentration with sufficiently high spatial resolution, atom probe field-ion microscopy (APFIM) was used.

II. EXPERIMENTAL

A. *Alloy and Heat Treatment*

An Fe-1.84C-3.84Si-2.95Mn (at. pct) steel was used for the present study. This steel had been studied previously[15] and is known to produce a negligible amount of retained austenite on quenching, making it ideal for this study. Alloys were initially homogenized at 1200 °C for 3 days in a sealed silica glass with an Ar atmosphere. The steel was rolled into 0.5 to 0.8 mm sheets and 3-mm-diameter discs were punched out from this sheet for transmission electron microscopy (TEM) specimens. The field-ion microscopy (FIM) samples were prepared from 0.5 × 0.5 mm square rods. They were austenitized at 1080 °C in an Ar atmosphere for 15 minutes and then quenched into ice water to form martensite. These were tempered with various conditions, as shown in Table I. Coates[4] assumed that the local equilibrium condition would be maintained when the diffusion distance was above 50 Å and the paraequilibrium would take control when it was below 10 Å. He calculated the diffusion distance from the velocity of transformation interface and diffusivity of substitutional elements as

$$\textit{diffusion distance} = \frac{2D_X}{\textit{interface velocity}} \qquad [1]$$

where D_X is the diffusivity of a substitutional element X (X = Mn and Si). As the interface velocity of transformation was not available, the random walk distance ($2\sqrt{D_{Mn} \cdot t}$) was used for approximating the diffusion distance of Mn (Table I). As seen from this table, the growth with the paraequilibrium mode is expected for heat treatment (HT)1 and HT2 and local equilibrium for HT3 to HT5 conditions.

B. *Microstructure and Compositional Analysis*

All tempered specimens were observed by a transmission electron microscope, PHILIPS* CM12, for preliminary characterization of the microstructure. The TEM samples were prepared using the standard twin-jet electropolishing technique. The atom probe analyses were performed by a time-of-flight atom probe FIM; the details of this instrument are described elsewhere.[16] The FIM tips were prepared by the standard two-step electropolishing technique.[17] The FIM images were observed with Ne as an imaging gas at 50 to 70 K, and the analyses were carried out with 15 pct pulse fraction (V_p/V_{dc})

*PHILIPS is a trademark of Philips Electronic Instruments Corp., Mahwah, NJ.

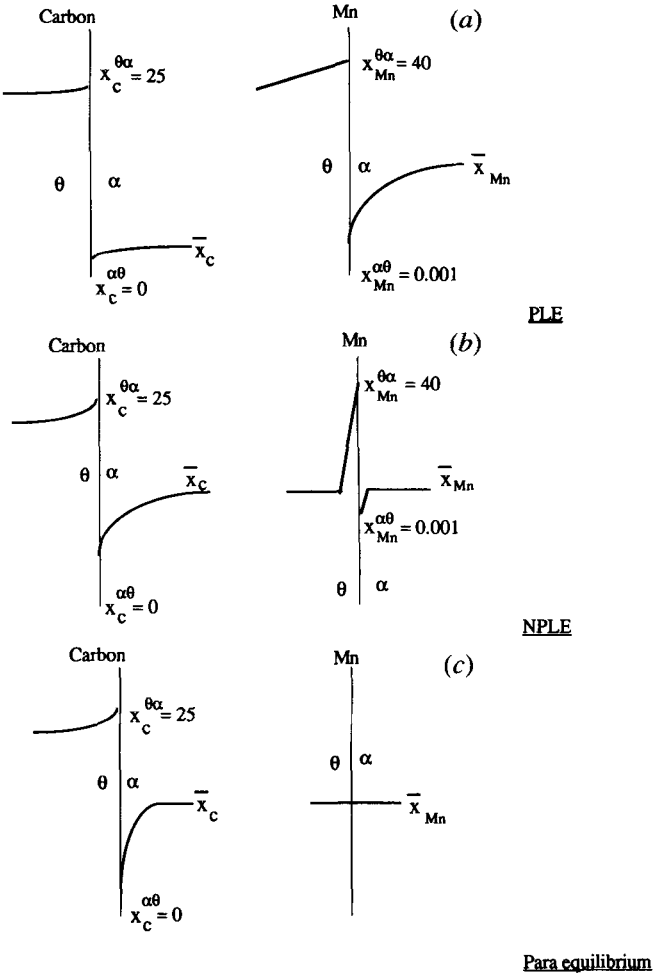

Fig. 1 — Schematic illustration of the concentration-depth profiles for the diffusional growth of cementite from martensite while tempering. The horizontal axis corresponds to distance and the vertical axis to concentration. The concentrations given in this figure are equilibrium concentrations (note that these concentrations are not calculated interface concentrations; nevertheless, the interface concentrations should be close to these values) calculated by the MTDATA program[12] for Fe-1.84C-3.84Si-2.95Mn (at. pct) steel tempered at 350 °C.

Table I. Heat-Treatment Conditions and Estimated Diffusion Distance Values

Heat Treatment	Temperature (°C)	Time (s)	≈Mn Diffusion Distance* (Å)
HT1	350	1.80×10^3	1.7
HT2	400	1.80×10^3	9.0
HT3	350	6.48×10^5	32.1
HT4**	450	5.40×10^3	98.3
HT5	500	0.30×10^3	54.8

*The diffusivity value was taken from Refs. 13 and 14.
**This heat treatment is two-step heat treatment (*i.e.*, after HT3, the sample was tempered at 450 °C).

under 10^{-8} torr Ne. In drawing the concentration-depth profile from APFIM data, 100 ions were treated as one block with a moving average of 50 ions. Carbon mass peaks corresponding to C^{++}, C^{+}, C_3^{++}, C_2^{+}, and C_3^{+} ions were considered for C concentration measurement.

III. RESULTS

A. *Early Stages of Tempering*

The transmission electron micrograph of the martensite tempered at the HT1 condition is shown in Figure 2. It shows the presence of cementite in lath martensite. The orientation relationship of the cementite with the ferrite is close to that of Bagaryatskii or Isaichiv type:

$$(101)_\alpha \| (100)_\theta \text{ and } (\bar{1}01)_\alpha \| (011)_\theta$$

Similar orientation relationships have also been reported in lower bainite.[18] In addition to the cementite, the faint spots[19] suggest the presence of a small amount of ε carbide that might have formed during heating, before the cementite formation. The matrix is observed with high dislocation density. The dark-field image using one of the variants of (111) cementite reflections shows the distribution of cementite. The cementite is in the form of thin platelets of 20-nm size. The samples after HT3 treatment (Figure 3) also show similar microstructure. The APFIM analyses were carried out for the specimens tempered with various conditions, as shown in Table I.

Figure 4(a) shows an FIM image of the alloy tempered at the HTI condition. On the basis of the preliminary TEM observation, the darkly imaging region indicated by arrowheads is believed to be cementite. Selected-area analysis clearly showed that the C concentration is significantly higher in this region. However, the concentration of the substitutional elements was found to be 3.3 ± 0.5 at. pct Si and 2.4 ± 0.4 at. pct Mn. These values are close to the nominal composition of the alloy, and hence, it is concluded that there was neither enrichment of Mn nor depletion of Si in the cementite at this stage. Figure 4(b) shows a concentration-depth profile of the same sample. In this figure, the presence of carbide can be clearly recognized from the abrupt change of the C concentration. The apparent concentration of C in the carbide determined by this analysis is only 16 ± 4 at. pct; however, we believe that this is due to an artificial effect during the atom probe analysis. In earlier atom probe works on steels, apparent low-C concentrations of cementite were also reported.[20,21] Nevertheless, atom probe results clearly show the presence of carbide in the concentration-depth profile with excellent spatial resolution. Furthermore, it gives relatively quantitative data regarding the substitutional elements such as Mn and Si. This plot clearly shows that the cementite formed without redistribution of Si and Mn. There were neither diffusion spikes nor segregation peaks of Si and Mn at the

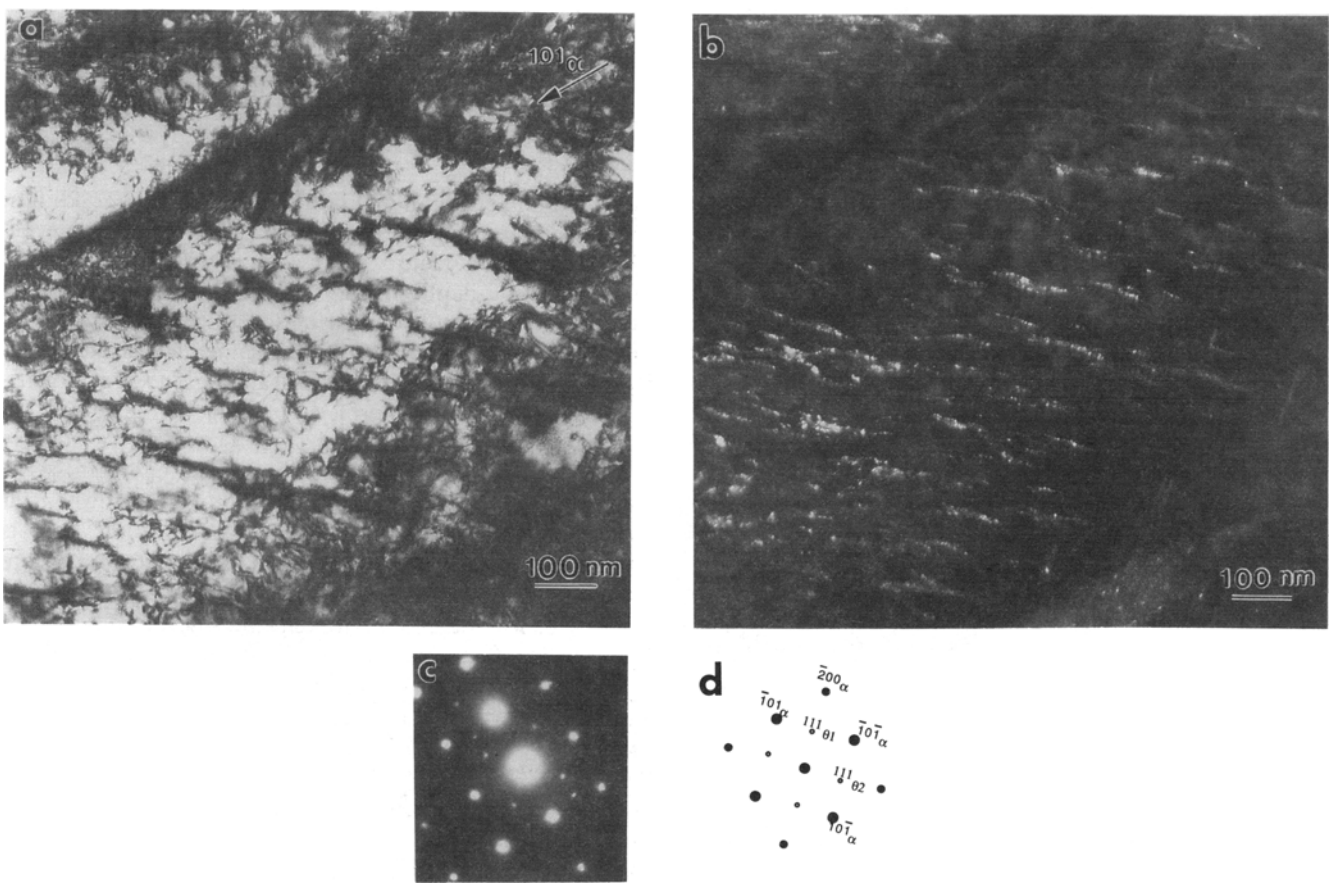

Fig. 2—HT1 condition: (*a*) bright-field TEM image showing the lath martensite structure with dispersed cementite; (*b*) dark-field image using one variant of $(111)_{\theta 1}$ cementite reflection in the same area; (*c*) selected-area diffraction pattern; and (*d*) schematic representation of the diffraction pattern.

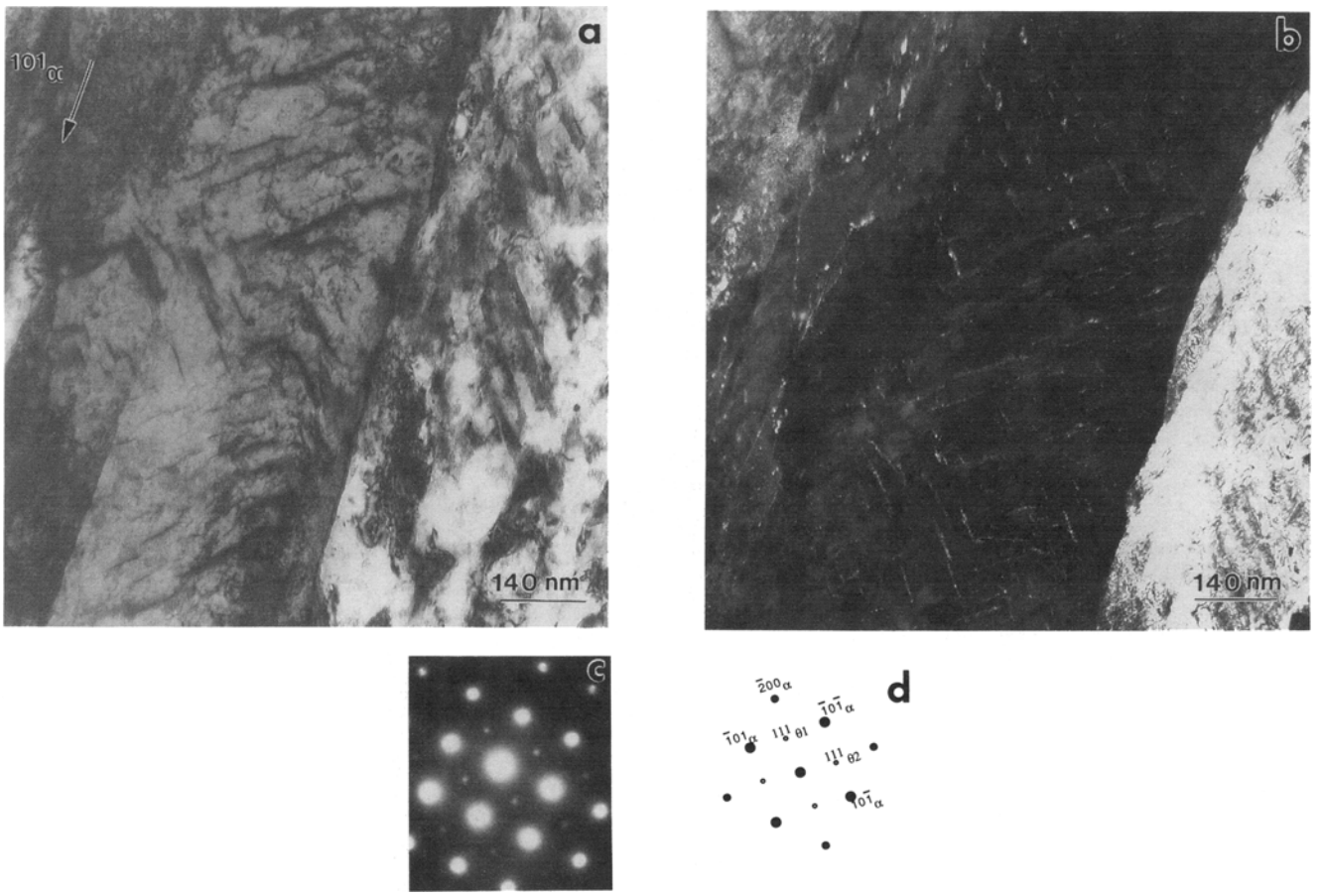

Fig. 3—HT3 condition: (*a*) bright-field TEM image showing the lath martensite structure with dispersed cementite; (*b*) dark-field image using one variant $(111)_{\theta 1}$ cementite reflection in the same area; (*c*) selected-area diffraction pattern; and (*d*) schematic representation of the diffraction pattern.

interface. An integral concentration-depth profile or a ladder plot shown in Figure 4(c) demonstrates the local concentration at the θ/α' interface more clearly, where the numbers of detected solute elements are plotted as a function of the total number of detected atoms; hence, the slope of the plot corresponds to the local concentration of the specimen. If there is any sharp concentration spike of Si and Mn during growth, a corresponding change in the slope of the Si and Mn curves should be observed. However, no segregation or partitioning of Si and Mn are observed. Similar analysis for the HT2 condition is shown in Figures 5(a) and (b). The ladder plot does not show any indication of the concentration change of Si and Mn in the cementite. The absence of partitioning and interfacial segregation of substitutional elements strongly suggests that the cementite formed by the paraequilibrium mode during the early stage of tempering below 400 °C.

B. *Extended Tempering*

Extended tempering treatments were carried out to observe the transition from paraequilibrium to local equilibrium. From the diffusion distance data (Table I), significant diffusion of the substitutional element is expected for the HT3 to HT5 conditions. Figure 6(a) shows an FIM image of the sample from the HT3 condition. Dimly imaging regions indicated by arrowheads are believed to be cementite, as in the case of Fig. 4(a). The concentration-depth profile (Figure 6(b)) of this sample does not show gross redistribution of Si and Mn yet. In contrast, the ladder plot from the same data (Figure 6(c)) shows the initiation of small-scale Si and Mn redistribution near the θ/α interface. Just outside the cementite, the slope of the ladder plot of Si seems to be slightly higher than the other area. Corresponding to this, the slope of the Si concentration is significantly lower near the interface in the cementite. This ladder plot suggests that Si is depleted in the cementite but enriched in ferrite near the interface. Manganese seems to be slightly enriched inside the cementite near the interface.

In order to enhance the redistribution of Mn and Si, HT4 and HT5 treatments were carried out. Note that HT4 is a two-step tempering, *i.e*, samples were tempered first at 350 °C for 6.48×10^5 s and then tempered at 450 °C for 5.4×10^3 s. This tempering was carried out in order to obtain a high-density cementite for facilitating the atom probe analysis. The concentration-depth profiles and ladder plots from the HT4 and HT5 conditions are shown in Figure 7 and 8, respectively. Both the ladder plot and the concentration-depth profiles

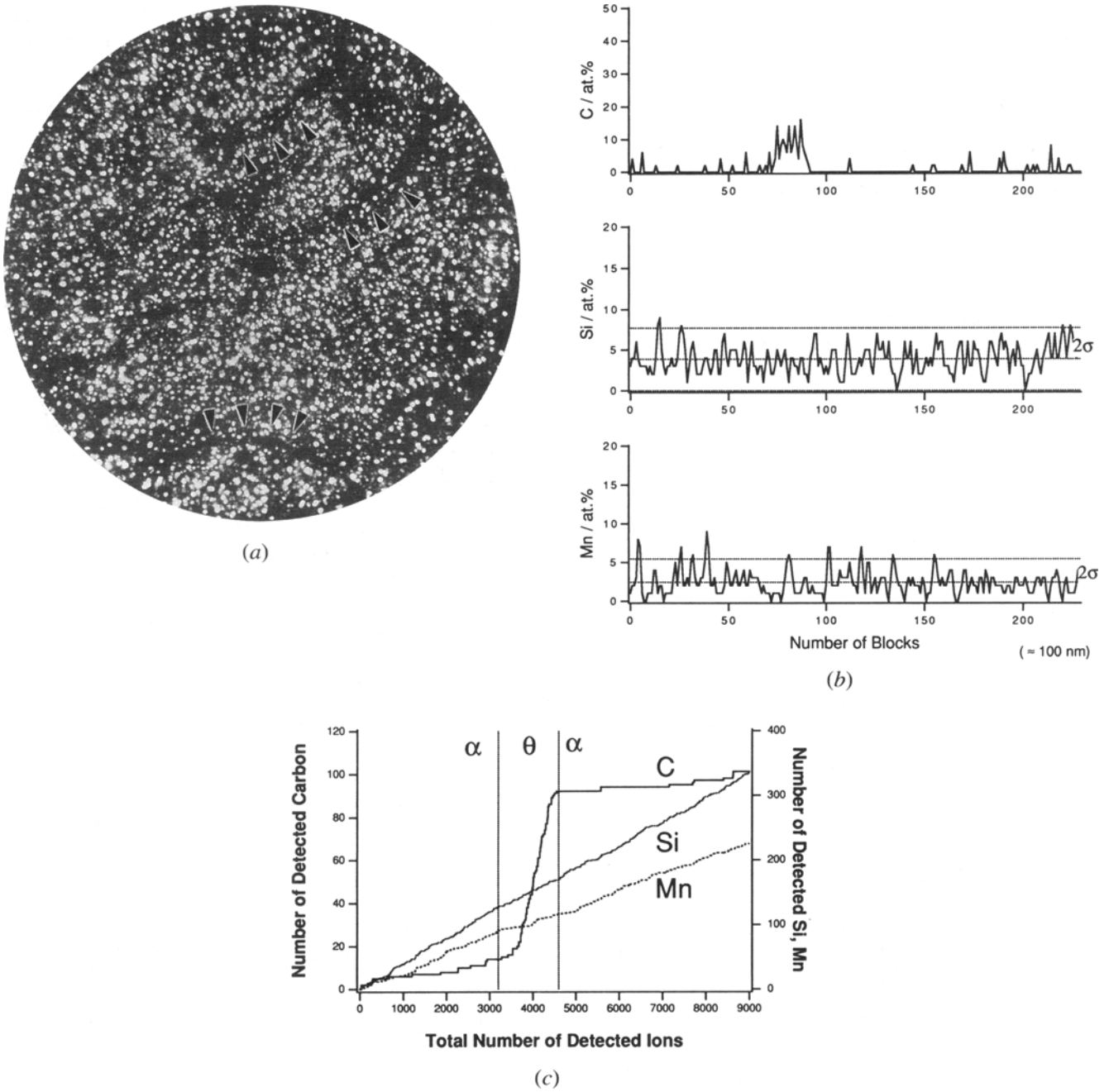

Fig. 4—(*a*) FIM image of the tempered martensite with the HT1 condition (the darkly imaging region corresponds to the cementite phase); (*b*) concentration depth profile; and (*c*) a ladder plot of the tempered martensite with the HT1 condition.

from the HT4 and HT5 conditions show extensive redistribution of Mn into cementite. The compositions of Si and Mn measured from cementite and ferrite are summarized in Table II. It is important to note that even after 1.5 hours at 450 °C, the redistribution of Si and Mn between cementite ferrite and ferrite was not complete. The cementite still contained 1.9 to 2.0 at. pct Si.

C. *As-Quenched Stage*

In order to understand the precipitation mechanism of cementite, the as-quenched martensite steel was also analyzed. Figure 9 shows a concentration-depth profile obtained from the as-quenched alloy. As reported previously by Taylor *et al.*,[22,23] the fluctuation of C concentration is present. While the overall C concentration of the alloy is only 1.84 at. pct, the maximum concentration of C reaches 10 at. pct. Such high C concentration peaks cannot be the statistical noise which is commonly observed in atom probe data. While the fluctuations of C concentration are clearly observed, Si and Mn seem to distribute homogeneously in the supersaturated solid solution. This indicates that the fluctuations occur only in C concentration.

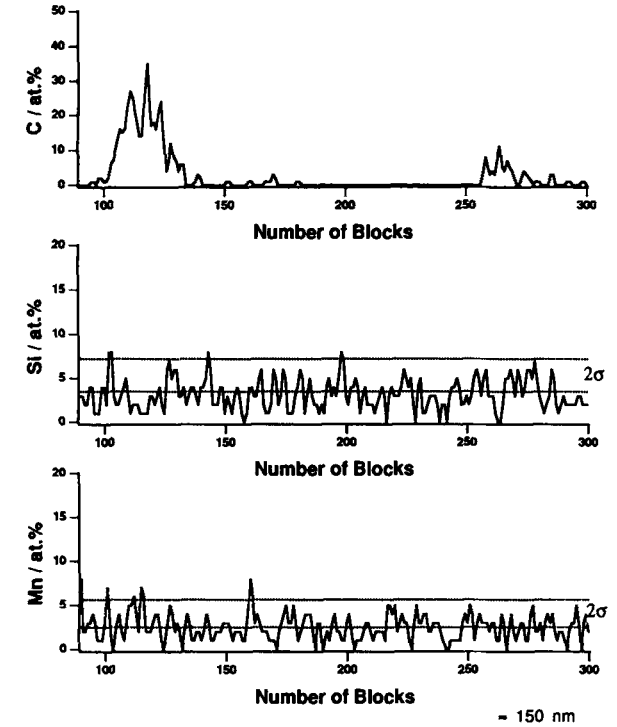

(*a*)

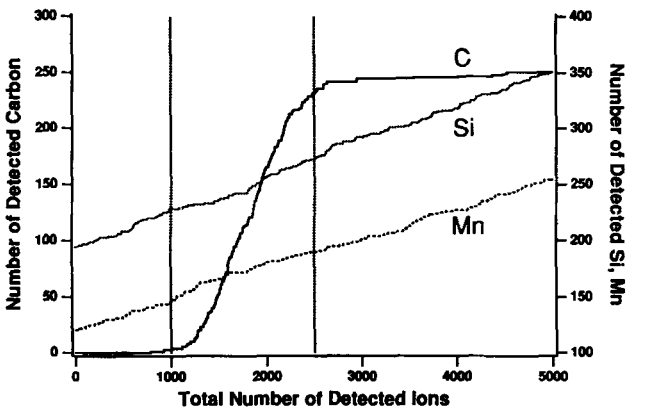

(*b*)

Fig. 5—(*a*) Concentration-depth profile and (*b*) a ladder plot of the tempered martensite with the HT2 condition. The dotted lines in (b) indicate the position of the cementite/ferrite interface.

III. DISCUSSION

A. *Early Stages of Tempering*

Since no partitioning was observed in the early stage of tempering (HT1 and HT2 conditions), it appears that the cementite precipitation and growth are controlled by the C diffusion alone. Because the atom probe analyses failed to detect concentration spikes of substitutional elements at the θ/α' interface, it is most likely that the cementite growth occurs by paraequilibrium mode in the early stage of tempering. The formation of paracementite was postulated as early as the 1950s,[7] and thereafter, many theoretical kinetic models were presented.[2–6] The present results directly show that the early-stage precipitation of cementite is indeed progressing in the paraequilibrium mode as predicted earlier. The diffusion distance for the HT1 conditions can be estimated from the observed thickness of the cementite plates (around 20 nm) and the growth time for 1.80×10^3 seconds. The diffusion distance calculated using Eq. [1] is 0.0072 Å, which is far less than the interatomic spacing. Thus, the paraequilibrium mode of growth appears to be reasonable under the HT1 condition. It is worthwhile to mention that Chang and Smith[24] had already shown that the ε carbide precipitation did not accompany the partitioning of substitutional elements during the early-stage tempering. However, the present result showed for the first time that the same thing is applicable to the early precipitation process of cementite. Also, the present work is the first direct evidence for the paraequilibrium growth of cementite.

Sherman *et al.*[25] measured the activation energy for carbide growth during martensite tempering. They attributed it to the pipe diffusion of Fe and substitutional atoms along a high density of dislocations which are present in the as-quenched martensite. If such diffusion controls the growth of the cementite in the present case, significant redistribution of Si and Mn should occur. However, the atom probe did not detect such redistribution of Si and Mn.

In general, reconstructive transformation is associated with rigorous atom movement at the interphase interface that causes the lattice change from parent phase to product. Thus, a concept of the paraequilibrium mode in reconstructive growth needs further consideration. It is interesting that reconstructive growth of cementite occurs without any redistribution of Fe and substitutional atoms at both sides of the interfaces. It has been suggested that the paraequilibrium mode of growth may be associated with only displacive transformation.[11] Andrews[26] showed that the cementite lattice can be formed by small zigzag movements of Fe atoms in a martensite lattice, similar to a displacive atom shuffle. Recently, Taylor *et al.*[22,23] suggested the mechanisms of carbide formation from martensite as follows. Initially, the C concentration fluctuations develop by spinodal decomposition at room temperature and the C-enriched and depleted regions are formed. Such high C-enriched regions undergo invariant plane strain (IPS) or shear to form transition carbides of orthorhombic structure. They also showed that the carbides exhibited extensive faulting on the basal plane.[23] Sandvik[27] also observed faulting in carbides which form from austenite and concluded that the carbides may form by a shear. As IPS is a conservative deformation with respect to the martensite matrix, no intrinsic movement of Fe or substitutional atoms is required, and hence, no partitioning is expected.

The concentration-depth profile of the as-quenched martensite (Figure 9) clearly shows the presence of C-enriched regions in the as-quenched condition, which agrees with the previous atom probe results of Fe-Ni-C martensite.[22] Such a fluctuation of C concentration may be associated with either spinodal decomposition[22] or C redistribution to dislocations in martensite.[28] Irrespective of the mechanism, C-enriched regions exist in the martensite phase in the as-quenched condition. These

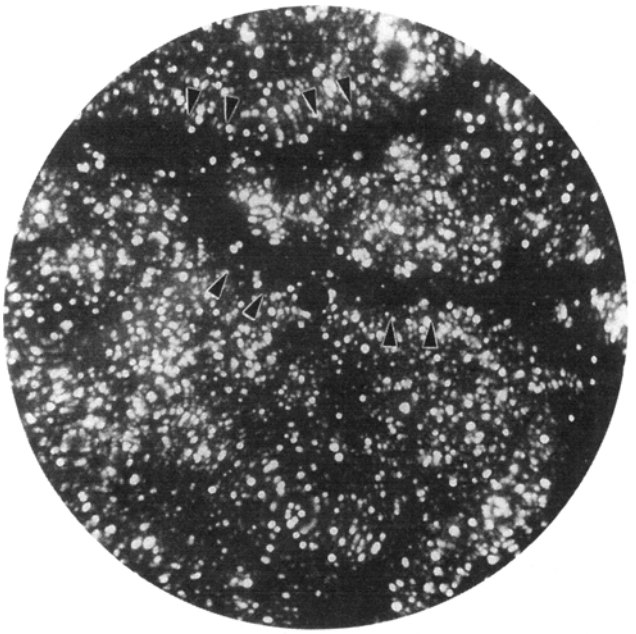

(a)

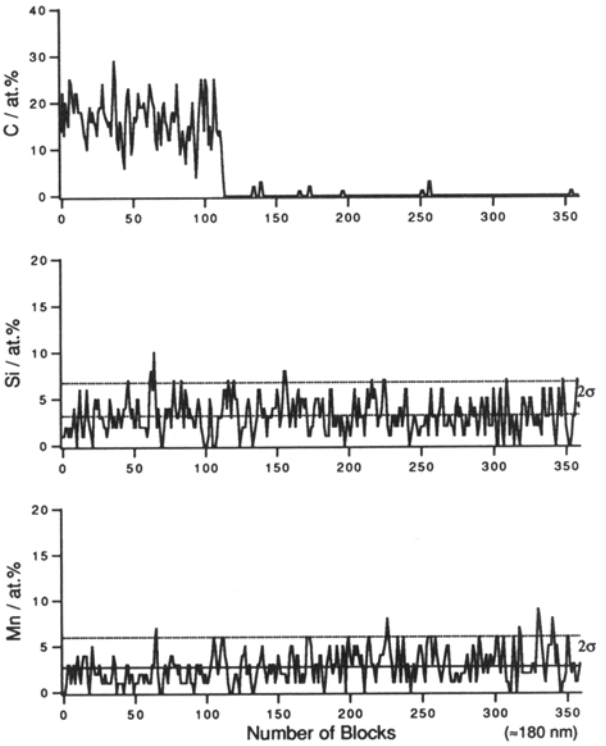

(b)

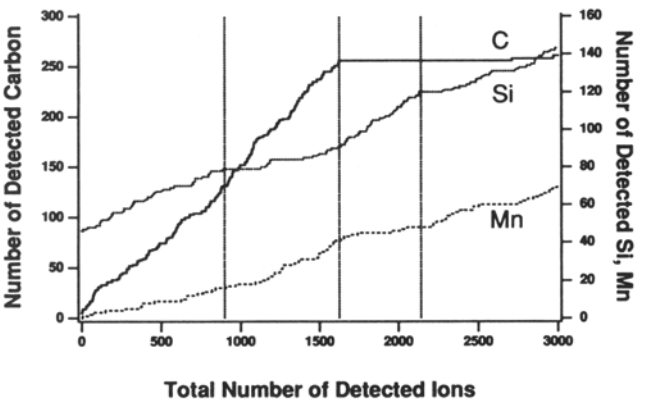

(c)

Fig. 6—HT3 condition: (*a*) Ne field-ion image, (*b*) concentration-depth profile, and (*c*) ladder plot of a tempered martensite with the HT3 condition. These indicate the onset of small-scale redistribution of Si and Mn. The dotted lines in (c) indicate the region of redistribution.

C-enriched regions may transform into carbide by displacive mode on heating to higher temperatures as suggested by Taylor *et al.*[23] Further work is necessary to extend the displacive mechanism of carbide precipitation to explain the absence of partitioning of substitutional elements in the early stage. Detailed crystallographic analysis, characterization of cementite substructure, and surface-relief analysis are needed to support the notion of a displacive mode of growth. It will be interesting to extend the present work to the cementite that precipitates in the lower bainitic steels.

B. *Extensive Tempering*

The partitioning behavior observed in the later stages of tempering (HT3, HT4, and HT5) is indeed expected. Similar partitioning has been studied previously using atom probe. Chang and Smith[24] and Bernard *et al.*[29] studied ε carbide and cementite which were formed during tempering of an Fe-C-Si steel. They showed that there was no enrichment of Si in the ε carbide. In addition, they found that cementite growth was controlled by Si diffusion in matrices in the later stages of tempering. They observed a Si-enriched region near the ferrite (α) and cementite (θ) interface and negligible amounts of Si in cementite. The present results are in line with these previous works. The composition data shown in Table II apparently show that the redistribution of Mn into cementite is faster than that of Si into ferrite. The measured redistribution is related to equilibrium partitioning of Mn and Si between cementite and ferrite.

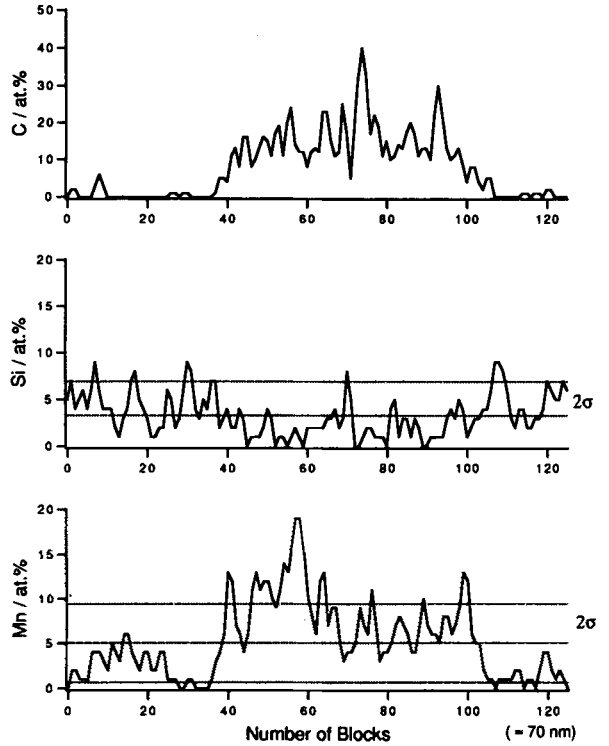

(*a*)

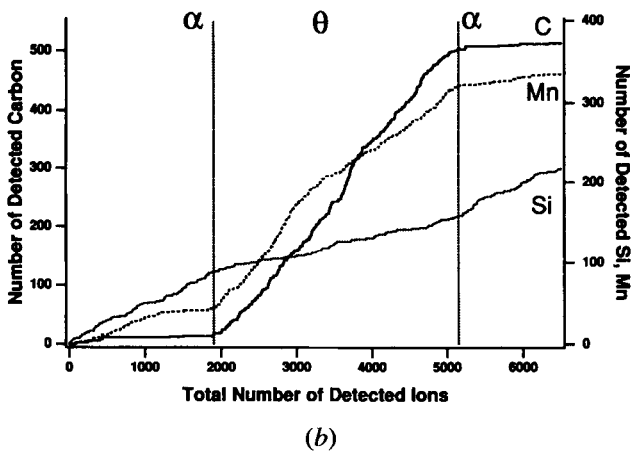

(*b*)

Fig. 7—(*a*) Concentration-depth profile and (*b*) ladder plot of a tempered martensite with the HT4 condition. The extensive partitioning of Si and Mn between ferrite and cementite can be observed.

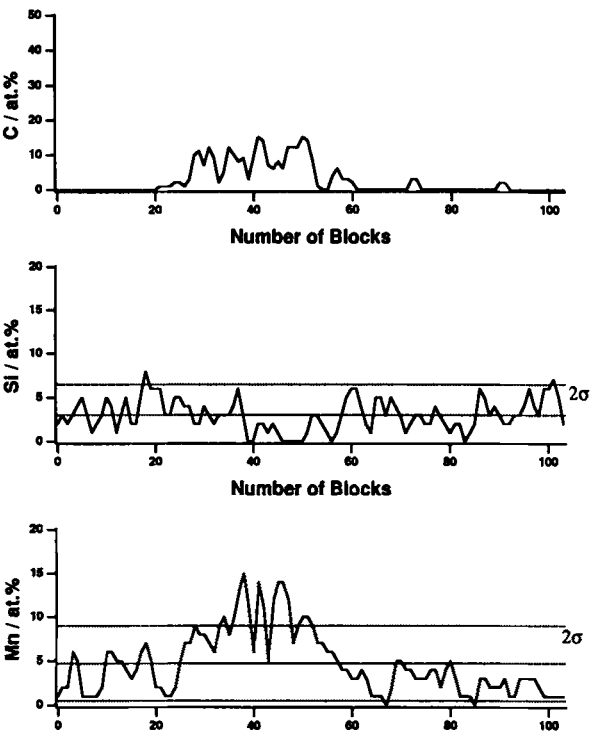

(*a*)

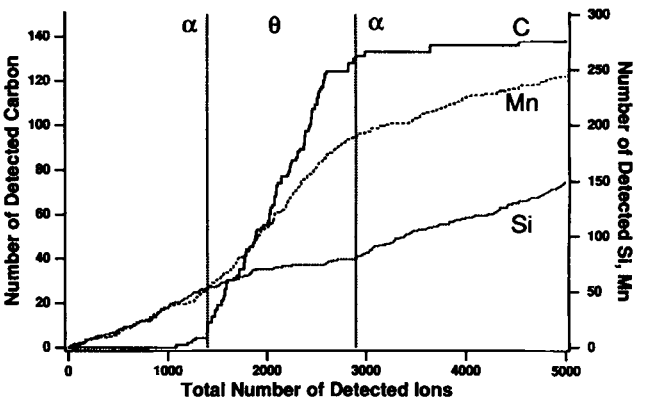

(*b*)

Fig. 8—(*a*) Concentration-depth profile and (*b*) ladder plot of a tempered martensite with the HT5 condition. The partitioning similar to HT4 condition can be clearly observed.

The calculated partitioning of Si in ferrite in equilibrium with cementite is only 4.1 at. pct in comparison to the nominal alloy concentration of 3.84 at. pct. The calculated partitioning of Mn into cementite is about 30 to 40 at. pct. It is also known that the solubility of Mn in cementite is quite high, as Mn_3C is known to be isomorphous with Fe_3C.[30] Thus, complete depletion of Si from cementite will be rather slower than the Mn enrichment in cementite. The presence of diffusion profiles of Mn and Si within the cementite phase indicates that the redistribution is not complete yet. Further extensive tempering is necessary to obtain equilibrium partitioning.

A significant difference in Si and Mn concentrations between the cementite and matrix is detected in the HT3,

Table II. Measured Nominal Concentration of Si and Mn in Ferrite and Cementite after Various Tempering Heat Treatments

Phase	Heat Treatment	Si/At. Pct	Mn/At. Pct
Cementite	HT3 (350/180 h)	2.75 ± 0.4	2.7 ± 0.4
Ferrite*		3.7 ± 0.5	2.5 ± 0.4
Cementite:	HT4 (350/180 h–450/1.5 h)	2.00 ± 0.25	8.6 ± 0.5
Ferrite		4.60 ± 0.5	2.0 ± 0.4
Cementite	HT5 (500/5 min)	1.9 ± 0.77	9.7 ± 1.67
Ferrite		4.9 ± 1.13	1.9 ± 0.7

*The composition quoted is near the interface of cementite and ferrite, in the ferrite matrix.

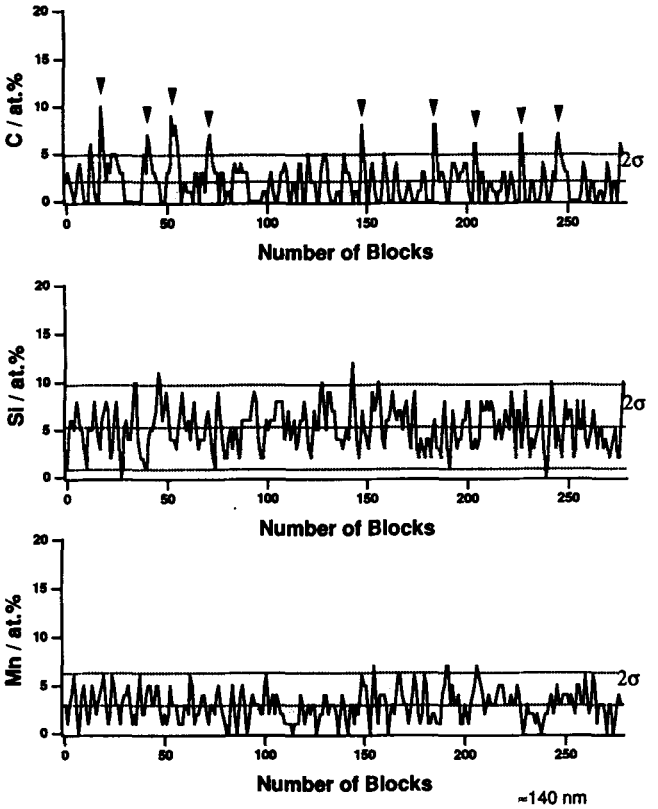

Fig. 9—Concentration-depth profile obtained from the as-quenched sample. The C-enriched regions are marked with arrowheads. There is no associated concentration fluctuation of Si and Mn, and the figure shows only the statistical fluctuations of Si and Mn.

HT4, and HT5 conditions. This means that the cementite growth is no longer in the paraequilibrium mode. The concentration-depth profiles from HT3 to HT5 can be considered as a transition stage from paraequilibrium to the PLE mode.[9] The composition profiles measured from HT3 can be taken as the initiation of the redistribution stage between PLE mode of growth and the attainment of equilibrium concentration at the interface. The composition profiles from the HT4 and HT5 conditions indicate the well-developed stage of redistribution that will eventually lead to equilibrium concentration at the interface.

V. CONCLUSIONS

The compositional analysis from atom probe indicates that the cementite growth is controlled by paraequilibrium C diffusion during early stages of tempering. In the as-quenched martensite, a significant fluctuation of C concentration was observed while the concentration of Si and Mn looked more or less uniform. It is likely that these C-enriched regions work as nucleation sites for cementite. By tempering the sample for an extended period of time or at higher temperatures, a clear indication of partitioning of Mn in cementite and Si in ferrite was observed. In these intermediate redistribution stages, concentration-depth profiles showed gradual change toward equilibrium concentrations at the interphase interface. This suggests that the growth mode changes as follows: paraequilibrium → local equilibrium.

The present result shows the importance of kinetic constraints such as gross difference in diffusivity in modeling the transformations in steels.

ACKNOWLEDGMENTS

The authors thank Dr. H.K.D.H. Bhadeshia, University of Cambridge, United Kingdom, for providing the specimens and for his encouragement in this work. Thanks are also due to Dr. R. Thompson, University of Cambridge, United Kingdom, for calculating the equilibrium partitioning for this alloy with the MTDATA program and to Dr. R.C. Reed, Imperial College, London, United Kingdom, for valuable comments on this article. The authors also acknowledge valuable discussions with Professor M. Enomoto, Ibaraki University, Hitachi, Japan.

REFERENCES

1. M. Hillert: *Internal Report*, Swedish Institute of Metal Research, Stockholm, 1953.
2. J.S. Kirkaldy: *Can. J. Phys.*, 1958, vol. 36, pp. 899-925.
3. G.R. Purdy, D.H. Weichert, and J.S. Kirkaldy: *Trans. TMS-AIME*, 1964, vol. 230, pp. 1025-34.
4. D.E. Coates: *Metall. Trans.*, 1972, vol. 3, pp. 1203-12.
5. D.E. Coates: *Metall. Trans.*, 1973, vol. 4, pp. 1077-86.
6. D.E. Coates: *Metall. Trans.*, 1973, vol. 4, pp. 2313-25.
7. A. Hultgren: *Jernkontorets Ann.*, 1951, vol. 135, p. 403.
8. H.K.D.H. Bhadeshia: *Prog. Mater. Sci.*, 1985, vol. 29, pp. 321-86.
9. J.B. Gilmour, G.R. Purdy, and J.S. Kirkaldy: *Metall. Trans.*, 1972, vol. 3, pp. 3213-22.
10. M. Enomoto and H.I. Aaronson: *Metall. Trans. A*, 1987, vol. 18A, pp. 1547-57.
11. H.K.D.H. Bhadeshia: *J. Phys. Colloq.*, 1989, vol. 50, pp. 389-94.
12. MTDATA, Metallurgical and Inorganic Thermodynamic Bank, National Physical Laboratory, Teddington, United Kingdom, 1989.
13. J. Kucera and Karel Stransky: *Mater. Sci. Eng.*, 1982, vol. 52, pp. 1-38.
14. J. Fridberg, L.E. Torndahl, and M. Hillert, *Jernkontorets Ann.*, 1969, vol. 153, pp. 263-76.
15. H.K.D.H. Bhadeshia and D.V. Edmonds: *Mater. Sci.*, 1979, vol. 13, pp. 325-34.
16. K. Hono, T. Hashizume, and T. Sakurai: *Surf. Sci.*, 1992, vol. 266, pp. 506-12.
17. M.K. Miller and G.D.W. Smith: *Atom Probe Microanalysis: Principles and Applications to Materials Problems*, Materials Research Society Pittsburgh, PA, 1989.
18. Y. Ohmori: *Mater. Trans. J. Inst. Met.*, 1989, vol. 30, pp. 487-97.
19. Y. Ohmori and I. Tamura: *Metall. Trans. A*, 1992, vol. 23A, pp. 2737-51.
20. M.K. Miller, P.A. Beaven, S.S. Brenner, and G.D.W Smith: *Metall. Trans. A*, 1983, vol. 14A, pp. 1021-24.
21. W. Sha and G.D.W. Smith: *Surf. Sci.*, 1992, vol. 266, pp. 416-23.
22. K.A. Taylor, L. Chang, G.B. Olson, G.D.W. Smith, M. Cohen, and J.B. Vander Sande: *Metall. Trans. A*, 1989, vol. 20A, pp. 2717-37.
23. K.A. Taylor, G.B. Olson, M. Cohen, and J.B. Vander Sande: *Metall. Trans. A*, 1989, vol. 20A, pp. 2749-65.
24. L. Chang and G.D.W. Smith: *J. Phys.*, 1984, vol. 45, pp. 397-401.
25. A.M. Sherman, G.T. Eldis, and M. Cohen: *Metall. Trans. A*, 1983, vol. 14A, pp. 995-1005.
26. K.A. Andrews: *Acta Metall.*, 1963, vol. 11, pp. 939-46.

27. B.P.J. Sandvik: *Metall. Trans. A*, 1982, vol. 13A, pp. 789-800.
28. Y. Ohmori and I. Tamura: *Metall. Trans. A*, 1992, vol. 23A, pp. 2147-58.
29. S.J. Barnard, G.D.W. Smith, A.J. Garret-Reed, and J. Vander Sande: *Proc. Intl. Conf. on Solid-Solid Phase Transformations*, H.I. Aaronson, D.E. Laughlin, R.F. Sekerka, and C.M. Wayman, eds., TMS-AIME, Warrendale, PA, 1981, pp. 881-85.
30. W. Hume-Rothery and G.V. Raynor: *The Structure of Metals and Alloys*, Monograph and Report Series, Institute of Metals, London, 1956, vol. 1, p. 270.